


Article

In Situ Synthesis of CsPbX₃/Polyacrylonitrile Nanofibers with Water-Stability and Color-Tunability for Anti-Counterfeiting and LEDs

Yinbiao Shi ¹, Xiaojia Su ¹, Xiaoyan Wang ¹ and Mingye Ding ^{1,2,3,*} 

¹ College of Science, Nanjing Forestry University, Nanjing 210037, China; bdd@njfu.edu.cn (Y.S.); 2211110417@njfu.edu.cn (X.S.); wangxiaoyan@njfu.edu.cn (X.W.)

² Key Laboratory of Advanced Energy Materials Chemistry (Ministry of Education), Nankai University, Tianjin 300071, China

³ College of Engineering and Applied Sciences, State Key Laboratory of Analytical Chemistry for Life Science, National Laboratory of Micro-Structures, Nanjing University, Nanjing 210023, China

* Correspondence: myding@njfu.edu.cn

Abstract: Inorganic CsPbX₃ (X = Cl, Br, I) perovskite quantum dots (PQDs) have attracted widespread attention due to their excellent optical properties and extensive application prospects. However, their inherent structural instability significantly hinders their practical application despite their outstanding optical performance. To enhance stability, an in situ electrospinning strategy was used to synthesize CsPbX₃/polyacrylonitrile composite nanofibers. By optimizing process parameters (e.g., halide ratio, electrospinning voltage, and heat treatment temperature), all-inorganic CsPbX₃ PQDs have been successfully grown in a polyacrylonitrile (PAN) matrix. During the electrospinning process, the rapid solidification of electrospun fibers not only effectively constrained the formation of large-sized PQDs but also provided effective physical protection for PQDs, resulting in the improvement in the water stability of PQDs by minimizing external environmental interference. Even after storage in water for over 100 days, the PQDs maintained approximately 93.5% of their photoluminescence intensity. Through the adjustment of halogen elements, the as-obtained composite nanofibers exhibited color-tunable luminescence in the visible light region, and based on this, a series of multicolor anti-counterfeiting patterns were fabricated. Additionally, benefiting from the excellent water stability and optical performance, the CsPbBr₃/PAN composite film was combined with red-emitting K₂SiF₆:Mn⁴⁺ (KSF) on a blue LED (460 nm), producing a stable and efficient WLED device with a color temperature of around 6000 K and CIE coordinates of (0.318, 0.322). These results provide a general approach to synthesizing PQDs/polymer nanocomposites with excellent water stability and multicolor emission, thereby promoting their practical applications in multifunctional optoelectronic devices and advanced anti-counterfeiting.

Keywords: perovskite quantum dots; electrospinning; nanofibers; multicolor tunable emissions; water stability



Citation: Shi, Y.; Su, X.; Wang, X.; Ding, M. In Situ Synthesis of CsPbX₃/Polyacrylonitrile Nanofibers with Water-Stability and Color-Tunability for Anti-Counterfeiting and LEDs. *Polymers* **2024**, *16*, 1568. <https://doi.org/10.3390/polym16111568>

Academic Editors: Baturalp Yalcinkaya, Ipek Yalcin Enis and Fatma Yalcinkaya

Received: 10 May 2024

Revised: 28 May 2024

Accepted: 30 May 2024

Published: 1 June 2024



Copyright: © 2024 by the authors. Licensee MDPI, Basel, Switzerland. This article is an open access article distributed under the terms and conditions of the Creative Commons Attribution (CC BY) license (<https://creativecommons.org/licenses/by/4.0/>).

1. Introduction

Recently, inorganic cesium lead halide perovskite quantum dots (PQDs) with the molecular formula CsPbX₃ (X = Cl, Br, I) have undergone extensive research as promising next-generation optoelectronic materials due to their high photoluminescent quantum yield (PLQY), color-tunable luminescence, narrow emission bands and so on [1–4]. They have gained significant attention in applications such as anti-counterfeiting, photocatalysis, bioimaging, displays and lighting [5,6]. However, the instability of PQDs can be attributed to the lower formation energy and ionic character of chemical bonds, which render them highly sensitive to environmental factors (e.g., water, temperature or radiation), greatly limiting their practical applications in optoelectronics [7–9]. To enhance the stability

of PQDs, a series of encapsulation strategies, including PQDs/mesoporous silica [10], PQDs/metal-organic frameworks [11] and PQDs/glass composites [12], have been proposed. However, the synthesis and processing processes of these methods are complex and cumbersome, including mesoporous template synthesis, sol-gel preparation, sintering, etc., and are not suitable for large-scale fabrication. Electrospinning technology has garnered significant attention in recent years. In addition to its application in preparing basic films, it has been demonstrated as a simple and high-throughput process for producing polymer nanofibers with enhanced crystallinity [13,14]. Additionally, electrospun nanofibers can serve as effective substrates for functional materials such as metal nanoparticles and quantum dots. The spatially confined effect of electrospun nanofibers can effectively enhance the stability of quantum dots and suppress the occurrence of aggregation phenomena [15], making it a feasible technique for manufacturing perovskite nanofiber films. For example, Fan's group utilized a one-step emulsion electrospinning method to produce organic-inorganic hybrid perovskite nanocrystals/polymer nanofibers, exhibiting excellent stability even in humid conditions (>60%) and underwater [16]. Similarly, Chen's group employed electrospinning in the one-step fabrication of uniform luminescent nanofibers based on a perovskite core-shell structure, with the perovskite and polymer serving as the core and shell, respectively. These nanofibers retained 50% of their initial luminescent intensity after immersion in water for 48 h [17]. The aforementioned similar studies have indeed enhanced the stability of PQDs to some extent. However, their long-term stability in water fails to meet the requirements for underwater background applications.

In this study, the selection of polyacrylonitrile (PAN) as the polymer matrix is due to its excellent weather resistance, UV resistance and good water/thermal stability [18–20]. Furthermore, polymer fibers also have the advantages of having a high surface specific surface area, adjustable diameter and uniform topography [15,21]. Hence, CsPbX₃/PAN composite nanofibers have been successfully synthesized via an in situ electrospinning method, aiming to achieve the protection and preservation of CsPbX₃ PQDs. Furthermore, a systematic investigation was conducted on the influence of electrospinning parameters (e.g., applied voltage, halide ratio and heat treatment temperature) on the morphology, optical properties and chemical stability of CsPbX₃/PAN composite nanofibers. The advantage of this process lies in the rapid stretching and solidification of PAN nanofibers during the electrospinning process, which effectively restricts the generation of large-sized PQDs and provides strong protection for CsPbX₃ PQDs inside PAN polymers. Thus, the electrospun CsPbBr₃/PAN composite film maintained long-term high stability in water, retaining over 93.5% of the photoluminescence intensity for more than 100 days. In addition, the composite fiber film exhibited excellent multicolor luminescence (a tunable emission spectrum from blue to red and high color purity) by adjusting the proportion of the halogen element. Considering the outstanding stability and luminescence performance, combined with the simple and efficient electrospinning process that integrated CsPbX₃ PQDs with PAN nanofibers, a novel composite film material was formed. This significantly enhances the water and thermal stability of PQDs and provides new approaches and methods for their practical applications in advanced anti-counterfeiting and white LEDs.

2. Experimental Section

2.1. Materials and Chemicals

Lead bromide (PbBr₂, ≥99.0%), lead chloride (PbCl₂, ≥99.99%), lead iodide (PbI₂, ≥98.0%), cesium bromide (CsBr, ≥99.5%), cesium chloride (CsCl, ≥99.5%), cesium iodide (CsI, ≥99.5%), N,N-Dimethylformamide (DMF, ≥99.9%), dimethyl sulfoxide (DMSO, ≥99.8%) and polyacrylonitrile (PAN, Mw ≈ 150,000) were purchased from Aladdin (Shanghai, China). K₂SiF₆:Mn⁴⁺ (KSF) phosphor was obtained from ZK HaoYe DongGuan Material Technology Co., Ltd. (Dongguan, China). All the reagents were used without further purification.

2.2. Preparation of PQDs/PAN Nanofibers

Typically, 0.5 mmol of PbX_2 and 0.5 mmol of CsX ($X = \text{Br}, \text{I}$) were dissolved in 10 mL of DMF. Then, 1.0 g of PAN was added into the above mixture under stirring. To dissolve PbCl_2 and CsCl , 5 mL of DMSO and 5 mL of DMF were used to prepare a precursor solution. The synthesis of various PQDs/PAN composite nanofibers was accomplished via a uniaxial electrospinning technique. A stainless-steel needle with a size of 20 G was employed during the electrospinning process. A total volume of 10 mL of precursor spinning solution was delivered using an electric pump at a rate of 2 mL/h. A fixed voltage of 15 kV was applied, with the needle positioned 15 cm away from the receiving substrate. The electrospinning process lasted for 2.5 h. Finally, the CsPbX_3 /PAN composite nanofibers were dried in an oven at 60 °C for 1 h to eliminate any residual organic solvents.

2.3. Fabrication of WLED

Then, 0.1 g of $\text{K}_2\text{SiF}_6\text{:Mn}^{4+}$ (KSF) phosphor powder was thoroughly blended with 5 g of organosilica gel and continuously stirred for 3 h. The resulting solution mixture was carefully applied onto a blue LED chip ($\lambda = 460 \text{ nm}$), which was covered with a dried CsPbBr_3 /PAN composite film. The assembly underwent curing at 80 °C for 5 h.

2.4. Characterizations

X-ray diffraction patterns of samples were collected by using an X-ray diffractometer (XRD, Ultima IV, Rigaku, Tokyo, Japan). Scanning electron microscopy (SEM) was performed on a JSM-7600F (JEOL, Tokyo, Japan) electron microscope. Transmission electron microscopy (TEM) and high-resolution transmission electron microscopy (HRTEM) images were taken on a JEM-2100F (JEOL, Tokyo, Japan) transmission electron microscope equipped with an X-ray spectrometer detector. The fluorescence distribution was confirmed by a Leica LSM-710 (Zeiss, Oberkochen, Germany) laser scanning confocal microscope (LSCM). UV-vis absorption spectra were recorded by a PE Lambda-950 UV-vis-NIR spectrophotometer (PerkinElmer, Waltham, MA, USA). The photoluminescence (PL) spectra and decay lifetimes were measured on an Edinburgh FLS980 fluorescence spectrometer (Edinburgh, Edinburgh, UK). The luminescent photographs were taken by a Canon EDS 70D digital camera (Canon, Tokyo, Japan).

3. Results and Discussions

Figure 1a depicts a schematic illustration of the one-step uniaxial electrospinning process. Inside the syringe, a PAN mixed solution containing CsX and PbX_2 ($X = \text{Cl}, \text{Br}, \text{I}$) in varying proportions is injected. Subsequently, the mixed precursor solution is continuously ejected through a spinning needle (be applied with a fixed voltage) with a diameter of 0.51 mm (20 G specification). Simultaneously, a fixed negative voltage is applied to the receiving substrate to provide traction to the spinning solution, stretching it into nanofibers during solidification. Within this process (Figure 1b), the nanofibers act as miniature nanoreactors, where the crystallization of perovskite quantum dots occurs along with polymer solidification [21], and the rapid solidification of PAN during electrospinning imposes a constraint effect on quantum dots, suppressing their rapid growth in the absence of other ligands [22]. At the same time, the high voltage and large specific surface area of the nanofibers promote the rapid evaporation of DMF in a very short time [23]. In this process, the needle makes a reciprocating motion from left to right, and by adjusting the ratio between different halogens (Cl, Br, I), large-area, regular, multicomponent PQD nanofiber films can be prepared (Figure 1c–g). These CsPbX_3 /PAN composite nanofibers exhibit excellent foldability, allowing arbitrary folding and cutting, demonstrating significant potential in wearable displays and other flexible luminescent devices.

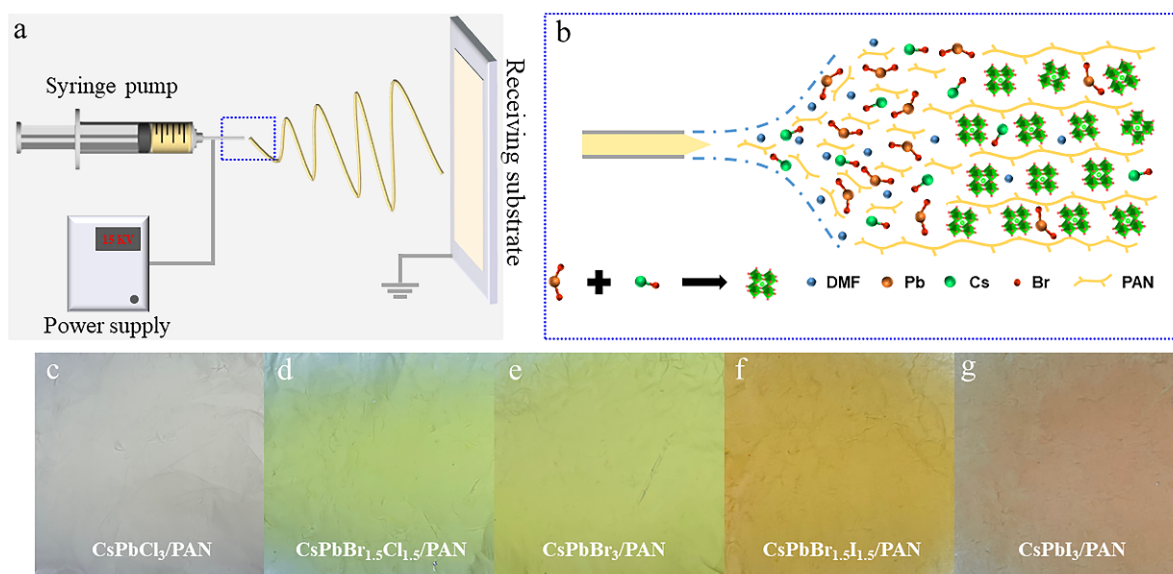


Figure 1. (a,b) Schematic of the one-step single-axis electrospinning setup to fabricate the perovskite light-emitting nanofibers. Photographs of as-synthesized $\text{CsPbX}_3/\text{PAN}$ samples: (c) $\text{CsPbCl}_3/\text{PAN}$, (d) $\text{CsPbBr}_{1.5}\text{Cl}_{1.5}/\text{PAN}$, (e) $\text{CsPbBr}_3/\text{PAN}$, (f) $\text{CsPbBr}_{1.5}\text{I}_{1.5}/\text{PAN}$, (g) $\text{CsPbI}_3/\text{PAN}$.

Firstly, the comprehensive morphological characterization of pure PAN and $\text{CsPbBr}_3/\text{PAN}$ composite nanofibers has been investigated, as shown in Figure 2. The pure PAN nanofibers exhibit uniform thickness and a smooth surface, with an average diameter of approximately 480 nm (Figure 2a,b). As illustrated in Figure 2c,d, the average diameters of $\text{CsPbBr}_3/\text{PAN}$ ($\text{CsBr}:\text{PbBr}_2$ is 1:1) composite nanofibers are around 350 ± 50 nm, indicating that these are finer fibers compared to pure PAN nanofibers. This is due to the addition of PQDS, which affects the arrangement and accumulation of pan molecules during fiber formation. And this results in a reduction in fiber diameter. Additionally, it can be observed that the surface of the nanofibers becomes slightly rougher, which may be attributed to residues of CsBr and PbBr_2 . Furthermore, the elemental mapping of the as-obtained composite nanofibers is provided in Figure 2e. From the figure, it is evident that the distribution of C, Pb and Br elements can be clearly observed along the as-obtained nanofibers. This confirms that PQDs are able to successfully grow inside nanofibers. Laser confocal fluorescence microscopy was then utilized for the random testing of $\text{CsPbBr}_3/\text{PAN}$ composite nanofibers (Figure 2f,g). The images show the distribution and physical dimensions of electrospun fibers under bright-field conditions and actual fluorescence images under 385 nm excitation. Merging the images under bright-field and fluorescence conditions reveals that all fibers in $\text{CsPbBr}_3/\text{PAN}$ electrospun fibers exhibit clear and uniform fluorescence. Finally, an XRD characterization test was conducted on $\text{CsPbBr}_3/\text{PAN}$ composite nanofibers to further investigate their specific structures and compositions. As seen in Figure 2h, the characteristic diffraction peaks of $\text{CsPbBr}_3/\text{PAN}$ composite nanofibers align with the standard X-ray diffraction pattern of CsPbBr_3 (PDF#18-0364) and PAN (PDF#48-2119), where the diffraction angles $2\theta = 15.2^\circ$, 21.54° and 30.72° correspond to the (100), (110) and (200) crystal planes of the CsPbBr_3 perovskite cubic phase. These angles match well with the standard CsPbBr_3 cubic phase, and no other impurity phases are observed. The above comprehensive characterization analysis validates the feasibility of the in situ synthesis of PQDs nanofibers via electrospinning.

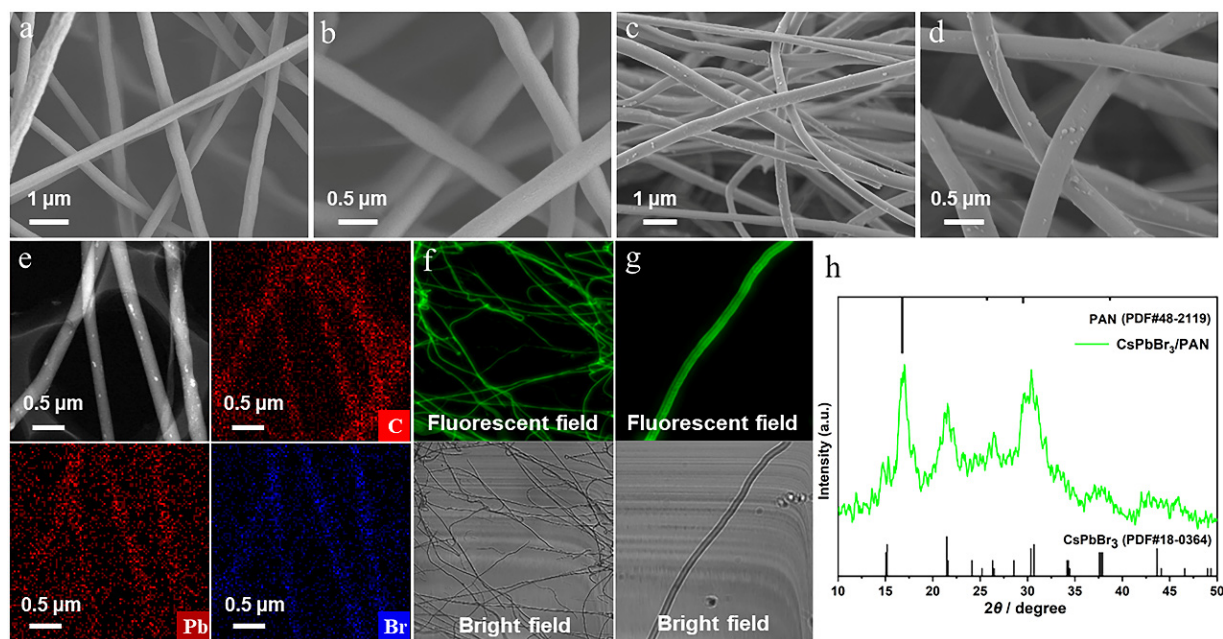


Figure 2. (a,b) SEM images of pure PAN nanofibers. (c,d) SEM images of CsPbBr₃/PAN (CsBr:PbBr₂ is 1:1) composite nanofibers. (e) TEM images of CsPbBr₃/PAN composite nanofibers. EDS mapping for C, Pb and Br elements. (f,g) Fluorescent field images and bright-field images of CsPbBr₃/PAN composite nanofibers recorded by LSCM, (h) XRD patterns of CsPbBr₃/PAN composite nanofibers.

Next, PL properties and chemical stability are displayed in Figure 3. Figure 3a illustrates the UV-vis absorption spectra and PL spectra of the CsPbBr₃/PAN composite nanofibers. The UV-visible absorption peak of this green film extends to around 525 nm, and it exhibits a PL peak at 512 nm with Full Width at Half Maximum (FWHM) of 24 nm. The inset in Figure 3a shows the actual emission photograph of the CsPbBr₃/PAN composite film under 365 nm UV excitation, vividly showcasing its bright and pure green fluorescence. Afterwards, the influence of adjustments in the CsBr/PbBr₂ ratio and applied voltage on the optical properties of PQDs/PAN composite nanofibers was investigated, employing CsPbBr₃/PAN as a representative example. CsPbBr₃/PAN composite nanofibers with different CsBr/PbBr₂ ratios were prepared under a voltage of 14 KV. As depicted in Figure 3b, variations in the CsBr/PbBr₂ ratio results in corresponding changes in the PL peak. As the CsBr/PbBr₂ ratio increases, the PL peaks are located at 514 nm, 511 nm, 512 nm, 506 nm and 518 nm, with corresponding FWHM values of 22 nm, 28 nm, 24 nm, 22 nm and 43 nm, respectively. Moreover, both an excessively high and low CsBr/PbBr₂ ratio can lead to a weakening of the PL intensity of sample. Additionally, under the condition where CsBr:PbBr₂ = 1:1, the variation in the PL intensity of CsPbBr₃/PAN composite nanofibers with different voltages is illustrated in Figure 3c. The PL intensity at 14 KV is twice that at 13 and 15 KV. However, with a further increase in voltage, the PL intensity begins to decrease. This is due to the intensified confinement growth effects in the nanofibers. At higher voltages, the polymer nanofibers solidify more rapidly, resulting in reduced growth time for PQDs within the nanofibers. This constrains the in situ growth of PQDs, leading to smaller particle sizes or limited crystallization. In order to achieve optimized process parameters, a systematic study was carried out on the halide ratios and applied voltages (Figures S1 and S2). From the comparison of emission spectra and PL intensity among various systems, it can be observed that when the CsBr:PbBr₂ is 1:1 and 3:2, composite nanofibers prepared under specific voltages exhibit the generation of spurious emission peaks. When the ratio is 4:1, the PL intensity of samples prepared at different voltages is relatively weak. Comprehensively taking into account its optical performance, the optimal process parameters are determined to be voltage, 14 KV; CsBr:PbBr₂ = 2:3.

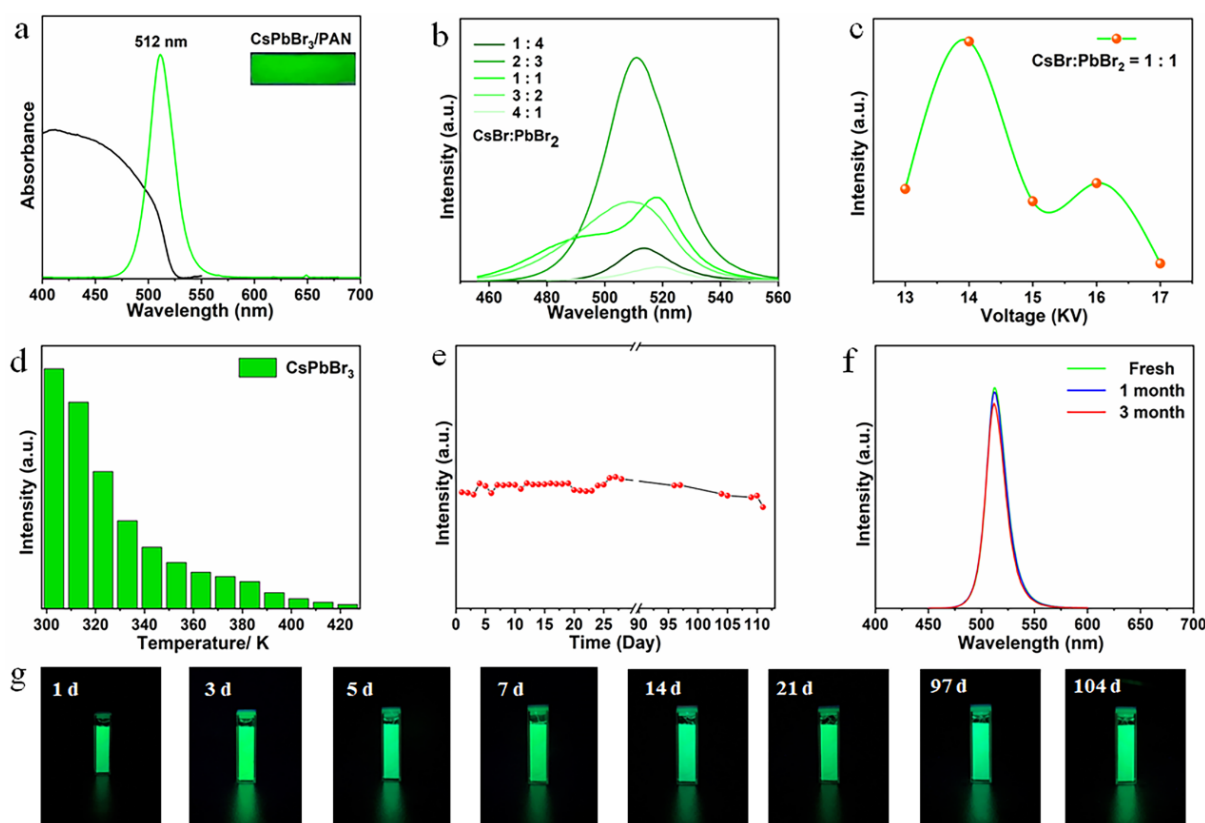


Figure 3. CsPbBr₃/PAN composite nanofibers: (a) UV-vis absorption and PL spectra. (b) Different ratios of CsBr and PbBr₂. (c) Different voltage. (d) Thermostability under 423 K. (e) Temporal evolution of PL intensity in room-temperature water. (f) Long-term storage stability. (g) Photos of CsPbBr₃/PAN composite nanofibers dipped in water for 1, 3, 5, 7, 14, 21, 97 and 104 days.

Under optimal ratios and voltage conditions, chemical stability assessments were performed on the prepared CsPbBr₃/PAN composite film. As observed in Figure 3d, with increasing temperature, the PL intensity of the prepared sample gradually decreases and quenches at 423 K, owing to the thermal quenching phenomenon. At elevated temperatures, the heightened exciton dissociation fosters direct interactions between electrons and phonons, thereby inducing fluorescence quenching. It is noteworthy that the PL emission peak position and FWHM remain essentially unchanged in the temperature range of 303–383 K (Figure S3), which ensures the color purity of the sample at high temperatures. This also reflects the superb optical performance of the CsPbBr₃/PAN composite nanofibers. Finally, long-term observations and tests were conducted on the stability and PL intensity decay of the CsPbBr₃/PAN composite film in water (completely immersed, with periodic water replenishment). Due to the encapsulation of PQDs within the polymeric matrix, the PL intensity of the CsPbBr₃/PAN composite film does not exhibit a significant decline for over 100 days (Figure 3e). Combining Figure 3f,g, the position and FWHM of its PL peak remain essentially unchanged. Under 365 nm excitation, the film continues to exhibit bright green fluorescence in water over an extended period. Consequently, polymeric nanofibers prepared through uniaxial electrospinning demonstrate exceptional encapsulation protection for in situ synthesized PQDs within the fibers.

Given the excellent optical performance and chemical stability of CsPbBr₃/PAN composite nanofibers, a mature electrospinning process strategy was employed to expand the preparation of PQDs/PAN composite nanofibers with different halogens, followed by a series of characterization tests. From Figure 4a–d, it can be seen that the nanofibers doped with four different halide elements exhibit uniform thickness. However, with the varying conductivity of the spinning solutions caused by different halide ions, there are significant

differences in the average diameter of the nanofibers. The diameters of CsPbCl₃/PAN, CsPbBr_{1.5}Cl_{1.5}/PAN, CsPbBr_{1.5}I_{1.5}/PAN and CsPbI₃/PAN composite nanofibers are approximately 400~800 nm; 200~300 nm; 100~200 nm; and 600~1000 nm, respectively. The specific structures and compositions of them are illustrated in Figure 4e. As Cl⁻ and I⁻ gradually substitute for Br⁻, changes in lattice size and interplanar spacing lead to a gradual shift in the overall characteristic peaks of the samples [24]. Notably, when preparing CsPbI₃/PAN composite nanofibers following the same procedure, the fluorescence emission spectrum appears chaotic (Figure S4a). To address this issue, annealing treatment was conducted. From Figure S4b, a significant enhancement in the red light emission peak is observed at an annealing temperature of 100 °C, and a single PL characteristic peak is achieved at 120 °C (Figure S4c). The effectiveness of this method is further demonstrated by comparing the actual luminescence images before and after annealing in Figure S4d–f. Building upon this, random site tests were conducted on the CsPbI₃/PAN composite nanofibers treated at 120 °C by using LSM (Figure S4g). Nanofibers exhibit bright and clear red fluorescence, which similarly confirms the effectiveness of the annealing treatment. The above phenomenon is caused by the short reaction time, leading to the immature crystallization of CsPbI₃ PQDs within freshly prepared nanofibers [25]. XRD comparative analysis in Figure 4e confirms that the characteristic diffraction peaks of CsPbI₃/PAN align with the standard diffraction pattern of the orthorhombic crystal structure (PDF#74-1970). This affirms the large-scale formation of CsPbI₃ PQDs within nanofibers.

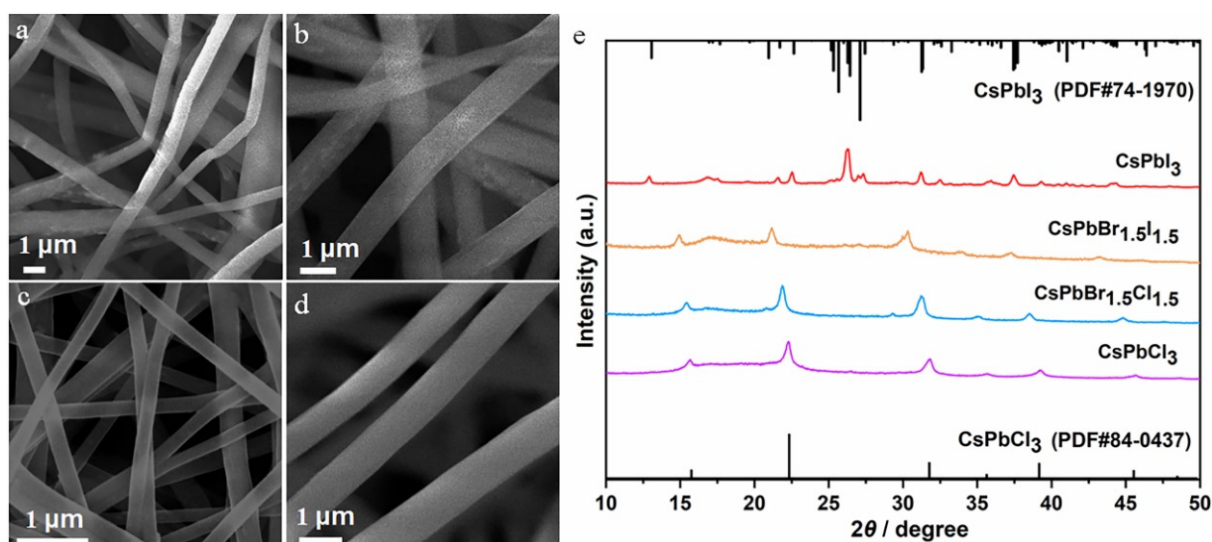


Figure 4. (a,b) SEM images of CsPbX₃/PAN composite nanofibers: (a) CsPbCl₃. (b) CsPbBr_{1.5}Cl_{1.5}. (c) CsPbBr_{1.5}I_{1.5}. (d) CsPbI₃. (e) XRD patterns of CsPbX₃/PAN composite nanofibers.

The UV-vis absorption spectra of the four multicolor CsPbX₃/PAN composite nanofibers are shown in Figure 5. The purple CsPbCl₃/PAN composite nanofiber (Figure 5a) exhibits a PL peak at 418 nm and a UV-visible absorption peak at 410 nm. The blue CsPbBr_{1.5}Cl_{1.5}/PAN composite nanofiber (Figure 5b) shows a PL peak at 454 nm and a UV-visible absorption peak at 448 nm. The orange CsPbBr_{1.5}I_{1.5}/PAN composite nanofiber (Figure 5c) displays a PL peak at 534 nm and a UV-visible absorption peak at 472 nm. Lastly, the red CsPbI₃/PAN composite nanofibers (Figure 5d) reveals a PL peak at 671 nm and a UV-visible absorption peak at 415 nm. By comparing the UV-vis absorption spectra of composite nanofibers composed of four different halogens, it can be observed that as the halide composition changes from Cl⁻ to I⁻, the CsPbX₃/PAN composite nanofibers exhibit higher absorbance in the ultraviolet and visible spectral regions [26]. Subsequently, thermal stability tests were conducted on the four aforementioned composite nanofiber films. The results indicated that samples doped with halogen element iodine exhibit excellent thermal stability (Figure S5).

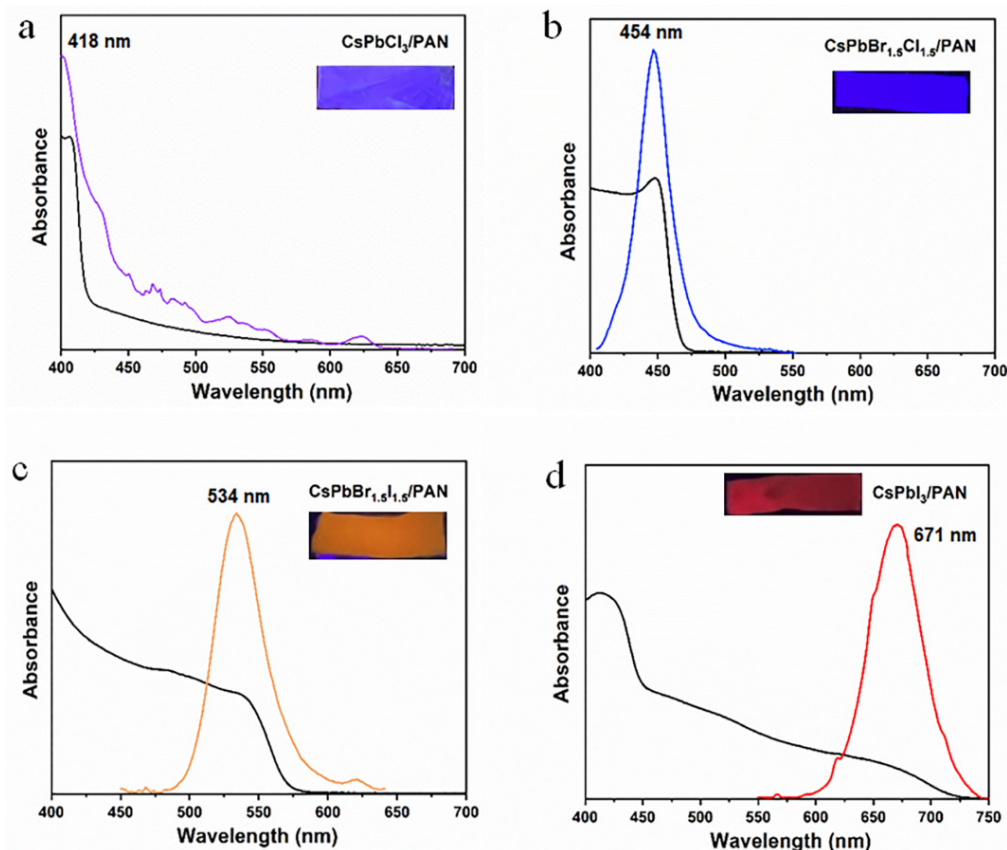


Figure 5. UV-vis absorption and PL spectra of CsPbX₃/PAN composite nanofibers (a) CsPbCl₃/PAN. (b) CsPbBr_{1.5}Cl_{1.5}/PAN. (c) CsPbBr_{1.5}I_{1.5}/PAN. (d) CsPbI₃/PAN.

Figure 6a illustrates the photoluminescence (PL) spectra of all CsPbX₃/PAN composite nanofibers, and their emitting wavelengths range from 418 to 671 nm. Unlike traditional cadmium-based QDs, the emission color of which is adjusted via the quantum size effect, the CsPbX₃/PAN composite nanofibers show the flexible tunability of emission color via simply modifying the PQD compositions. Figure 6b presents corresponding actual luminescent photographs under 365 nm ultraviolet excitation, displaying vivid and vibrant colors. Later, time-resolved single-photon counting spectroscopy was employed. From Figure 6c, it can be observed that the average PL lifetime of composite nanofibers prepared with halide elements Br and Cl doping is smaller than that of PQD nanofiber films doped with Br and Cl. (Table S1). This behavior aligns with PL decay patterns of PQDs reported in the literature [27–29]. As the halide atom radius increases at the X site (Cl[−] = 1.81 Å, Br[−] = 1.96 Å, I[−] = 2.20 Å), it leads to the enlargement of the bandgap of PQDs, thereby increasing the carrier recombination rate. On the other hand, different halide elements can induce changes in the band structure of PQDs, which may affect the formation and recombination rate of electron–hole pairs, consequently influencing the fluorescence lifetime [27]. The luminescent films of PQD nanofibers prepared by electrospinning differ significantly from traditional lanthanide-doped phosphors. CsPbX₃/PAN composite nanofibers, with their narrow FWHM and tunable emission, can generate saturated, single-color luminescence [30–32]. The CIE coordinates, as shown in Figure 6d, illustrate the broad color gamut of these CsPbX₃ PQDs (Table S2). Considering the excellent micolor emission properties and exceptional stability of the electrospun composite films, these samples hold great promise for multicolored optoelectronic applications in aquatic environments in applications of counterfeit prevention and LEDs.

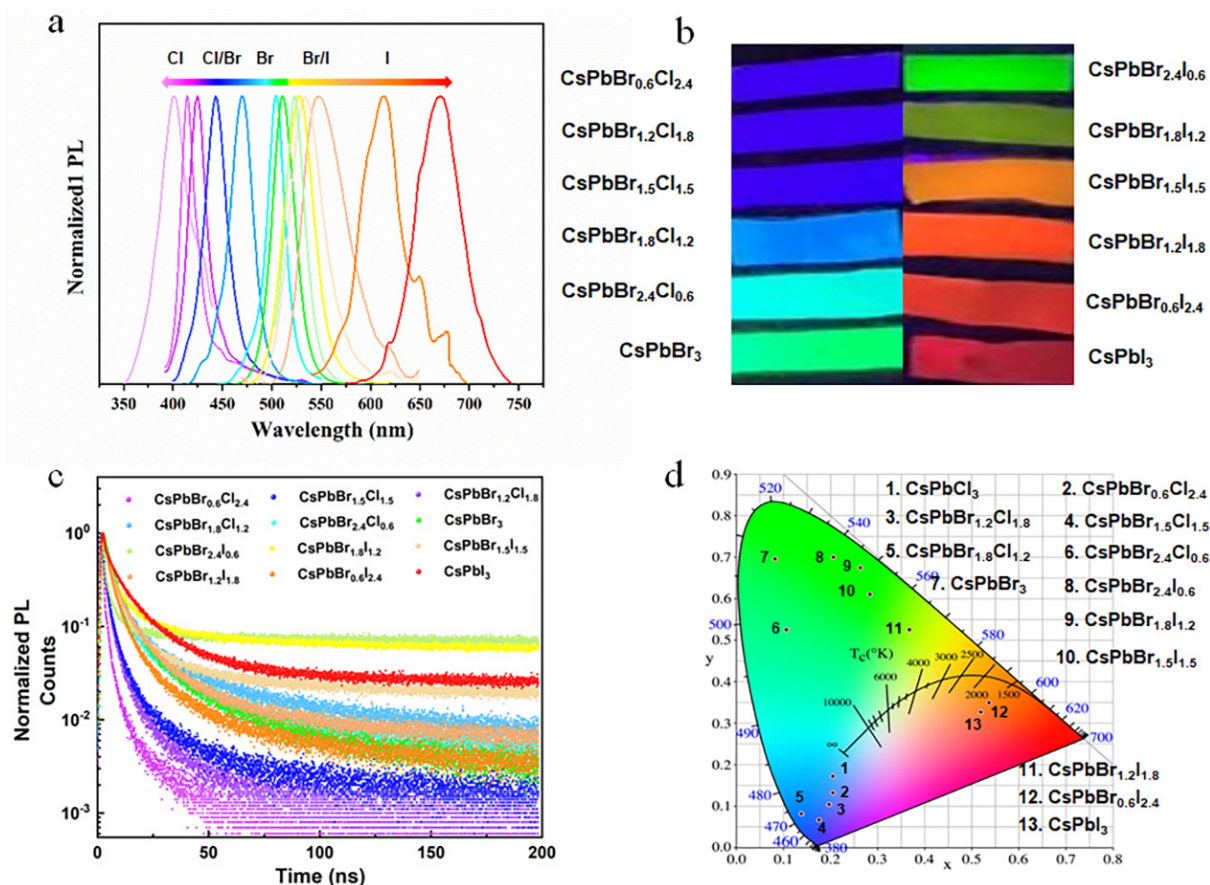


Figure 6. CsPbX₃/PAN composite nanofibers with different halogen constitutions: (a) PL spectra. (b) Digital photographs under UV excitation ($\lambda = 365$ nm). (c) PL decay curves. (d) CIE coordinate and color gamut.

On the one hand, electrospinning offers the advantage of producing large-area, highly stable fluorescent nanofiber films; on the other hand, the flexibility (Figure 7d,e) of the nanofibers themselves allows for arbitrary cutting and assembling into any desired pattern, which renders them suitable for applications in anti-counterfeiting and WLED [33,34]. Thus, leveraging the foldability of nanofiber films attempts to cut multicolor CsPbX₃/PAN composite films into different patterns (Figure 7). Figure 7a–c, respectively, show fluorescent patterns (a school badge and the letters NJFU) composed of individual multicolor CsPbX₃/PAN composite films created by cutting and assembling CsPbX₃/PAN composite films with various compositions under UV excitation ($\lambda = 365$ nm) in dark conditions. The excellent display performance implies potential applications in the field of multicolor anti-counterfeiting. This utilization of electrospun nanofiber films showcases promise for future advancements in multifunctional materials for security and display technologies.

Benefiting from the exceptional PL performance and good long-term stability of CsPbX₃/PAN composite nanofibers, white light-emitting diodes (WLEDs) were successfully fabricated using CsPbBr₃/PAN composite film and red-emitting KSF phosphors. Figure 8a illustrates the operational principles of the WLED, wherein a blue light-emitting diode (LED) emitting at a wavelength of 460 nm is selected as the excitation light source. The KSF and CsPbBr₃/PAN composite film are combined and overlaid onto the LED. Following this, they are encapsulated and cured with organic adhesive, which results in a simplified WLED device [35]. Performance testing of the prepared WLED under a 20 mA drive current, as shown in Figure 8b, reveals distinct emission peaks in the blue, green and red spectral ranges. The inset presents actual emission photographs of the WLED device, providing a clear depiction of its ability to emit bright, pure white light. Finally, based on Figure 8c, the WLED device exhibits CIE coordinates of (0.318, 0.322), placing it within

the white light region with a color temperature of approximately 6000 K [36]. Taking into account the chemical stability of the CsPbBr₃/PAN composite film, it shows significant potential in light-emitting devices.

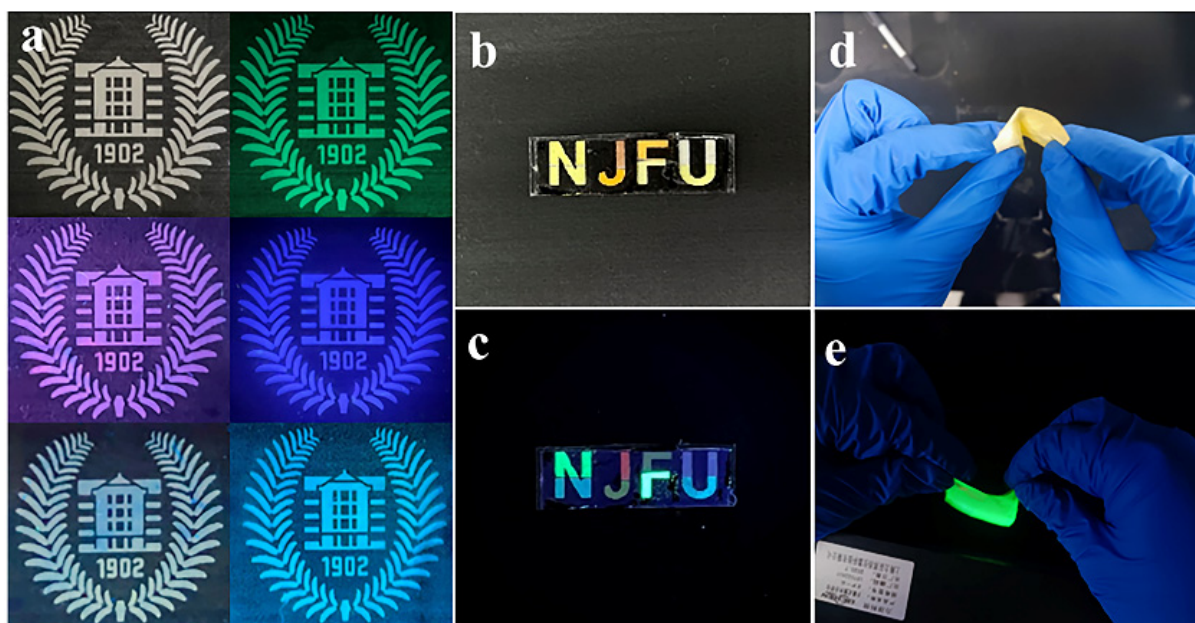


Figure 7. (a–c) Demonstration of the application of a multicolor fluorescent patterns for anti-counterfeiting. (d,e) Flexibility on display.

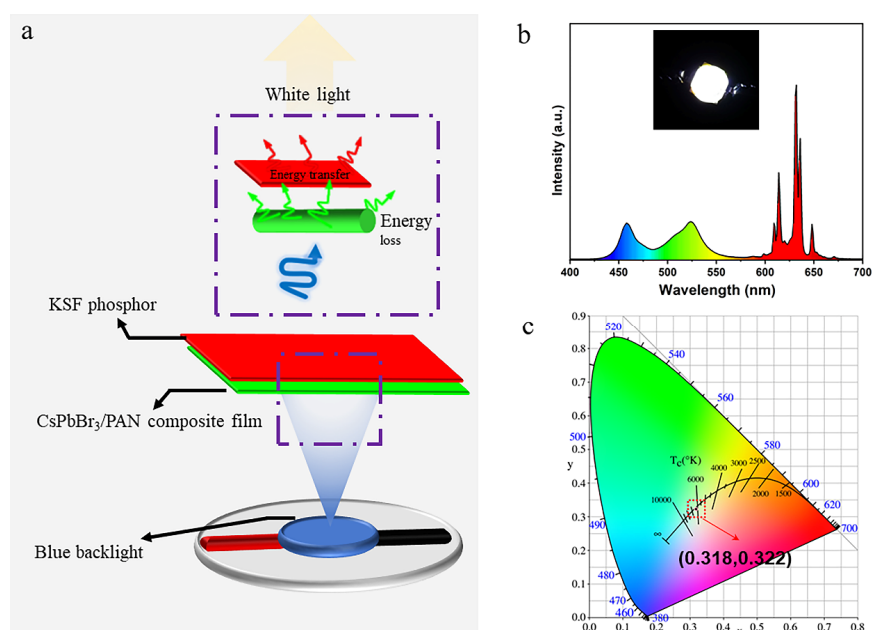


Figure 8. (a) Simplified structure of WLED. (b) EL spectrum (inset shows a digital camera image of the working WLED). (c) CIE coordinate and color gamut of WLED.

4. Conclusions

In summary, we employed an electrospinning in situ synthesis strategy to fabricate visible-light tunable CsPbX₃ (X = Cl, Br, I)/PAN composite nanofibers with emitting wavelengths ranging from 418 to 671 nm. Through process optimization, specific parameters were set as follows: voltage: 14 KV; CsBr:PbBr₂ = 2:3. The CsPbBr₃/PAN nanofiber film exhibited good stability in water resistance tests. This remarkable stability is attributed to

the effective encapsulation of PQDs by the polymeric matrix, which isolates them from the detrimental effects of oxygen and moisture. Even after immersion in water for over 100 days, the film maintained approximately 93.5% of its PL intensity. Building upon this, doping various halogen elements endowed it with multicolor luminescent properties. Combined with the flexibility of the composite films themselves, they can be fabricated into various shapes and multicolored anti-counterfeiting patterns. Furthermore, leveraging the narrow FWHM and tunable emission characteristics of CsPbX₃/PAN (X = Cl, Br, I) composite nanofibers, we successfully prepared a bright white light-emitting diode (WLED) with CIE coordinates of (0.318, 0.322) and a color temperature of around 6000 K under blue LED excitation. These results not only provide a unique approach for the synthesis of PQDs but also advance their practical applications in optoelectronic lighting and display technologies.

Supplementary Materials: The following supporting information can be downloaded at: <https://www.mdpi.com/article/10.3390/polym16111568/s1>, Figure S1: (a–e) PL spectra of CsPbBr₃/PAN composite nanofibers under different voltages and different ratios of CsBr and PbBr₂; Figure S2: (a–d) PL Intensity trend change chart of CsPbBr₃/PAN composite nanofibers under different voltages and different ratios of CsBr and PbBr₂; Figure S3: (a) Temperature-varying PL spectra of CsPbBr₃/PAN composite film. (b) PL peak positions and FWHM; Figure S4: (a–c) PL spectra of CsPbI₃/PAN composite nanofibers under different voltages and various thermal treatment temperatures. (d–f) Photos of CsPbI₃/PAN composite film under different voltages and various thermal treatment temperatures. (g) LSCM; Figure S5: Thermal stability of CsPbX₃/PAN composite nanofibers: (a) CsPbCl₃/PAN, (b) CsPbBr_{1.5}Cl_{1.5}/PAN, (c) CsPbBr_{1.5}I_{1.5}/PAN, (d) CsPbI₃/PAN; Table S1: Fluorescence lifetime of multicolor CsPbX₃/PAN composite nanofibers; Table S2: CIE coordinates of multicolor CsPbX₃/PAN composite nanofibers; Table S3: List of water stability tests. References [37–39] are cited in the supplementary materials.

Author Contributions: Conceptualization, M.D.; Methodology, Y.S., X.S. and Xiaoyan Wang; Formal analysis, X.W. and M.D.; Investigation, Y.S. and M.D.; Data curation, X.S.; Writing—original draft, Y.S.; Writing—review & editing, M.D.; Project administration, M.D.; Funding acquisition, M.D. All authors have read and agreed to the published version of the manuscript.

Funding: This study was financially supported by the Natural Science Foundation of Jiangsu Province (No. BK20211280).

Institutional Review Board Statement: “Not applicable” for studies not involving humans or animals.

Data Availability Statement: Data are contained within the article and Supplementary Information.

Conflicts of Interest: The authors declare that they have no known competing financial interests or personal relationships that could have appeared to influence the work reported in this paper.

References

1. Akkerman, Q.A.; Gandini, M.; Di Stasio, F.; Rastogi, P.; Palazon, F.; Bertoni, G.; Ball, J.M.; Prato, M.; Petrozza, A.; Manna, L. Strongly emissive perovskite nanocrystal inks for high-voltage solar cells. *Nat. Energy* **2016**, *2*, 16194. [[CrossRef](#)]
2. Lin, J.; Lu, Y.; Li, X.; Huang, F.; Yang, C.; Liu, M.; Jiang, N.; Chen, D. Perovskite Quantum Dots Glasses Based Backlit Displays. *ACS Energy Lett.* **2021**, *6*, 519–528. [[CrossRef](#)]
3. Swarnkar, A.; Chulliyil, R.; Ravi, V.K.; Irfanullah, M.; Chowdhury, A.; Nag, A. Colloidal CsPbBr₃ Perovskite Nanocrystals: Luminescence beyond Traditional Quantum Dots. *Angew. Chem. Int. Ed.* **2015**, *54*, 15424–15428. [[CrossRef](#)] [[PubMed](#)]
4. Yuan, Z.; Miao, Y.; Hu, Z.; Xu, W.; Kuang, C.; Pan, K.; Liu, P.; Lai, J.; Sun, B.; Wang, J.; et al. Unveiling the synergistic effect of precursor stoichiometry and interfacial reactions for perovskite light-emitting diodes. *Nat. Commun.* **2019**, *10*, 2818. [[CrossRef](#)] [[PubMed](#)]
5. Stephen, A.; Biju, A.; Sona, C.P.; Peediyekkal, J. Recent trends in synthesis, properties, and applications of CsPbX₃ quantum dots: A review. *J. Lumin.* **2024**, *269*, 120462. [[CrossRef](#)]
6. Shi, J.; Wang, Z.; Gaponenko, N.V.; Da, Z.; Zhang, C.; Wang, J.; Ji, Y.; Ding, Y.; Yao, Q.; Xu, Y.; et al. Stability Enhancement in All-Inorganic Perovskite Light Emitting Diodes via Dual Encapsulation. *Small* **2024**, *23*, 10478. [[CrossRef](#)] [[PubMed](#)]
7. Buin, A.; Pietsch, P.; Xu, J.; Voznyy, O.; Ip, A.H.; Comin, R.; Sargent, E.H. Materials Processing Routes to Trap-Free Halide Perovskites. *Nano Lett.* **2014**, *14*, 6281–6286. [[CrossRef](#)] [[PubMed](#)]
8. Kim, J.; Lee, S.-H.; Lee, J.H.; Hong, K.-H. The Role of Intrinsic Defects in Methylammonium Lead Iodide Perovskite. *J. Phys. Chem. Lett.* **2014**, *5*, 1312–1317. [[CrossRef](#)] [[PubMed](#)]

9. Song, S.; Lv, Y.; Cao, B.; Wang, W. Surface Modification Strategy Synthesized CsPbX₃ Perovskite Quantum Dots with Excellent Stability and Optical Properties in Water. *Adv. Funct. Mater.* **2023**, *33*, 2300493. [[CrossRef](#)]
10. Yu, X.; Wu, L.; Yang, D.; Cao, M.; Fan, X.; Lin, H.; Zhong, Q.; Xu, Y.; Zhang, Q. Hydrochromic CsPbBr₃ Nanocrystals for Anti-Counterfeiting. *Angew. Chem. Int. Ed.* **2020**, *59*, 14527–14532. [[CrossRef](#)]
11. Qiao, G.-Y.; Guan, D.; Yuan, S.; Rao, H.; Chen, X.; Wang, J.-A.; Qin, J.-S.; Xu, J.-J.; Yu, J. Perovskite Quantum Dots Encapsulated in a Mesoporous Metal–Organic Framework as Synergistic Photocathode Materials. *J. Am. Chem. Soc.* **2021**, *143*, 14253–14260. [[CrossRef](#)] [[PubMed](#)]
12. Sun, K.; Tan, D.; Fang, X.; Xia, X.; Lin, D.; Song, J.; Lin, Y.; Liu, Z.; Gu, M.; Yue, Y.; et al. Three-dimensional direct lithography of stable perovskite nanocrystals in glass. *Science* **2022**, *375*, 307–310. [[CrossRef](#)]
13. Chang, H.; Liu, C.; Chen, W. Flexible Nonvolatile Transistor Memory Devices Based on One-Dimensional Electrospun P3HT:Au Hybrid Nanofibers. *Adv. Funct. Mater.* **2013**, *23*, 4960–4968. [[CrossRef](#)]
14. Chen, J.Y.; Wu, H.C.; Chiu, Y.C.; Chen, W.C. Plasmon-Enhanced Polymer Photovoltaic Device Performance Using Different Patterned Ag/PVP Electrospun Nanofibers. *Adv. Energy Mater.* **2014**, *4*, 1301665. [[CrossRef](#)]
15. Chen, W.; Chen, L.; Liu, F.; Tsai, W.; Tung, B.; Venkatesan, M.; Tsai, M.; Lin, J.; Kuo, C. Perovskite-Nanocrystal-Doped Cellulose Nanocrystal Ligands for Electrospun Nanofibers with Excellent Stability. *Small* **2023**, *19*, e2207685. [[CrossRef](#)] [[PubMed](#)]
16. Wang, Z.; He, H.; Liu, S.; Wang, H.; Zeng, Q.; Liu, Z.; Xiong, Q.; Fan, H.J. Air Stable Organic–Inorganic Perovskite Nanocrystals@Polymer Nanofibers and Waveguide Lasing. *Small* **2020**, *16*, 2004409. [[CrossRef](#)]
17. Tsai, P.-C.; Chen, J.-Y.; Ercan, E.; Chueh, C.-C.; Tung, S.-H.; Chen, W.-C. Uniform Luminous Perovskite Nanofibers with Color-Tunability and Improved Stability Prepared by One-Step Core/Shell Electrospinning. *Small* **2018**, *14*, e1704379. [[CrossRef](#)] [[PubMed](#)]
18. Matysiak, W.; Tański, T.; Jarka, P.; Nowak, M.; Kępińska, M.; Szperlich, P. Comparison of optical properties of PAN/TiO₂, PAN/Bi₂O₃, and PAN/SbSI nanofibers. *Opt. Mater.* **2018**, *83*, 145–151. [[CrossRef](#)]
19. Razavi, N.; Neisiany, R.E.; Ayatollahi, M.R.; Ramakrishna, S.; Khorasani, S.N.; Berto, F. Fracture assessment of polyacrylonitrile nanofiber-reinforced epoxy adhesive. *Theor. Appl. Fract. Mech.* **2018**, *97*, 448–453. [[CrossRef](#)]
20. Tao, J.; Wang, Y.; Zheng, X.; Zhao, C.; Jin, X.; Wang, W.; Lin, T. A review: Polyacrylonitrile as high-performance piezoelectric materials. *Nano Energy* **2023**, *118*, 108987. [[CrossRef](#)]
21. Cheng, R.; Liang, Z.; Zhu, L.; Li, H.; Zhang, Y.; Wang, C.; Chen, S. Fibrous Nanoreactors from Microfluidic Blow Spinning for Mass Production of Highly Stable Ligand-Free Perovskite Quantum Dots. *Angew. Chem. Int. Ed.* **2022**, *61*, e202204371. [[CrossRef](#)] [[PubMed](#)]
22. Li, X.; Zhang, Y.; Zhang, L.; Xia, S.; Zhao, Y.; Yan, J.; Yu, J.; Ding, B. Synthesizing Superior Flexible Oxide Perovskite Ceramic Nanofibers by Precisely Controlling Crystal Nucleation and Growth. *Small* **2021**, *18*, 2106500. [[CrossRef](#)] [[PubMed](#)]
23. Xue, J.; Wu, T.; Dai, Y.; Xia, Y. Electrospinning and Electrospun Nanofibers: Methods, Materials, and Applications. *Chem. Rev.* **2019**, *119*, 5298–5415. [[CrossRef](#)] [[PubMed](#)]
24. Chen, D.; Chen, X.; Wan, Z.; Fang, G. Full-Spectral Fine-Tuning Visible Emissions from Cation Hybrid Cs_{1-m}FA_mPbX₃ (X = Cl, Br, and I, 0 ≤ m ≤ 1) Quantum Dots. *ACS Appl. Mater. Interfaces* **2017**, *9*, 20671–20678. [[CrossRef](#)] [[PubMed](#)]
25. Zheng, J.; Yue, G.; Zhou, Z.; Li, H.; Hou, L.; Sun, C.; Li, X.; Kang, L.; Wang, N.; Zhao, Y.; et al. Phase Transition Induced Thermal Reversible Luminescent of Perovskite Quantum Dots Fibers. *Adv. Funct. Mater.* **2023**, *33*, 2300607. [[CrossRef](#)]
26. Zheng, W.; Huang, P.; Gong, Z.; Tu, D.; Xu, J.; Zou, Q.; Li, R.; You, W.; Bunzli, J.-C.G.; Chen, X. Near-infrared-triggered photon upconversion tuning in all-inorganic cesium lead halide perovskite quantum dots. *Nat. Commun.* **2018**, *9*, 3462. [[CrossRef](#)] [[PubMed](#)]
27. Dou, Y.; Wang, S.; Zhang, C.; Luo, H.; Li, X.; Wang, H.; Cao, F.; Shen, P.; Zhang, J.; Yang, X. Ten-Gram-Scale Synthesis of FAPbX₃ Perovskite Nanocrystals by a High-Power Room-Temperature Ultrasonic-Assisted Strategy and Their Electroluminescence. *Adv. Mater. Technol.* **2020**, *5*, 1901089. [[CrossRef](#)]
28. Levchuk, I.; Osvet, A.; Tang, X.; Brandl, M.; Perea, J.D.; Hoegl, F.; Matt, G.J.; Hock, R.; Batentschuk, M.; Brabec, C.J. Brightly Luminescent and Color-Tunable Formamidinium Lead Halide Perovskite FAPbX₃ (X = Cl, Br, I) Colloidal Nanocrystals. *Nano Lett.* **2017**, *17*, 2765–2770. [[CrossRef](#)]
29. Minh, D.N.; Kim, J.; Hyon, J.; Sim, J.H.; Sowlih, H.H.; Seo, C.; Nam, J.; Eom, S.; Suk, S.; Lee, S.; et al. Room-Temperature Synthesis of Widely Tunable Formamidinium Lead Halide Perovskite Nanocrystals. *Chem. Mater.* **2017**, *29*, 5713–5719. [[CrossRef](#)]
30. Wang, Y.; Guo, N.; Shao, B.; Yao, C.; Ouyang, R.; Miao, Y. Adjustable photoluminescence of Bi³⁺ and Eu³⁺ in solid solution constructed by isostructural end components through composition and excitation-driven strategy. *Chem. Eng. J.* **2020**, *421*, 127735. [[CrossRef](#)]
31. Yadav, S.; Kumar, D.; Yadav, R.S.; Singh, A.K. Recent progress on optical properties of double perovskite phosphors. *Prog. Solid State Chem.* **2023**, *69*, 100391. [[CrossRef](#)]
32. Zhang, L.; Li, P.; Zhao, A.; Li, X.; Tang, J.; Zhang, F.; Jia, G.; Zhang, C. Synthesis, structure, and color-tunable luminescence properties of lanthanide activator ions doped bismuth silicate as single-phase white light emitting phosphors. *J. Alloys Compd.* **2020**, *816*, 152546. [[CrossRef](#)]
33. Wang, H.; Qian, X.; An, X. Introducing lanthanide metal–organic framework and perovskite onto pulp fibers for fluorescent anti-counterfeiting and encryption. *Cellulose* **2022**, *29*, 1115–1127. [[CrossRef](#)]

34. Tian, T.; Yang, M.; Fang, Y.; Zhang, S.; Chen, Y.; Wang, L.; Wu, W.-Q. Large-area waterproof and durable perovskite luminescent textiles. *Nat. Commun.* **2023**, *14*, 234. [[CrossRef](#)] [[PubMed](#)]
35. Xu, Y.; Lou, S.; Xia, C.; Xuan, T.; Li, H. Controllable synthesis of all inorganic lead halide perovskite nanocrystals and white light-emitting diodes based on CsPbBr₃ nanocrystals. *J. Lumin.* **2020**, *222*, 117132. [[CrossRef](#)]
36. Yang, C.; Niu, W.; Chen, R.; Pang, T.; Lin, J.; Zheng, Y.; Zhang, R.; Wang, Z.; Huang, P.; Huang, F.; et al. In Situ Growth of Ultrapure Green-Emitting FAPbBr₃-PVDF Films via a Synergetic Dual-Additive Strategy for Wide Color Gamut Backlit Display. *Adv. Mater. Technol.* **2022**, *7*, 2200100. [[CrossRef](#)]
37. Wei, S.; Zhu, H.; Zhang, J.; Wang, L.; An, M.; Wang, Y.; Zhang, X.; Liu, Y. Luminescent perovskite nanocrystal-epoxy resin composite with high stability against water and air. *J. Alloys Compd.* **2019**, *789*, 209–214. [[CrossRef](#)]
38. Ma, C.; Zhang, M.; Zhang, J.; Liao, J.; Sun, H.; Ji, D.; Pang, R.; Zhang, H.; Liu, J.; Liu, S. Highly Luminescent and Stable Perovskite Quantum Dots Films for Light-Emitting Devices and Information Encryption. *Adv. Funct. Mater.* **2024**, *23*, 16717. [[CrossRef](#)]
39. Hu, X.; Xu, Y.; Wang, J.; Ma, J.; Wang, L.; Jiang, W. In Situ Fabrication of Superfine Perovskite Composite Nanofibers with Ultrahigh Stability by One-Step Electrospinning Toward White Light-Emitting Diode. *Adv. Fiber Mater.* **2022**, *5*, 183–197. [[CrossRef](#)]

Disclaimer/Publisher’s Note: The statements, opinions and data contained in all publications are solely those of the individual author(s) and contributor(s) and not of MDPI and/or the editor(s). MDPI and/or the editor(s) disclaim responsibility for any injury to people or property resulting from any ideas, methods, instructions or products referred to in the content.